Food Chemistry: X 15 (2022) 100371

Contents lists available at ScienceDirect

Food Chemistry: X

journal homepage: www.sciencedirect.com/journal/food-chemistry-x

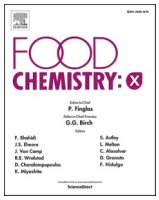

Spatially resolved metabolomics reveals variety-specific metabolic changes in banana pulp during postharvest senescence

Zhibin Yin [a,1], Tao Dong [b,1], Wenjie Huang [a,1], Mingyi Du [c], Dong Chen [c], Alisdair R. Fernie [d], Ganjun Yi [b,*], Shijuan Yan [a,*]

[a] Guangdong Key Laboratory for Crop Germplasm Resources Preservation and Utilization, Agro-biological Gene Research Center, Guangdong Academy of Agricultural Sciences, Guangzhou 510640, China
[b] Institute of Fruit Tree Research, Guangdong Academy of Agricultural Sciences, Key Laboratory of South Subtropical Fruit Biology and Genetic Resource Utilization (Ministry of Agriculture and Rural Affairs), Guangdong Province Key Laboratory of Tropical and Subtropical Fruit Tree Research, Guangzhou, 510640, China
[c] Key Laboratory of Natural Pesticide and Chemical Biology of the Ministry of Education, South China Agricultural University, Guangzhou 510642, China
[d] Max-Planck-Institute of Molecular Plant Physiology, Am Muhlenberg 1, Potsdam-Golm 14476, Germany

ARTICLE INFO

Keywords:
Banana
Mass spectrometry imaging
Metabolomics
Monoamine
Amino acid
Soluble sugars

ABSTRACT

Banana is one of most popular fruits globally due to health-promoting and disease-preventing effects, yet little is known about *in situ* metabolic changes across banana varieties. Here, we integrated gold nanoparticle (AuNP)-assisted laser desorption/ionization mass spectrometry imaging (LDI-MSI) and metabolomics to investigate the spatiotemporal distribution and levels of metabolites within Brazil and Dongguan banana pulps during postharvest senescence. Metabolomics results indicated that both postripening stages and banana varieties contribute to metabolite levels. Benefiting from improved ionization efficiency of small-molecule metabolites and less peak interference, we visualized the spatiotemporal distribution of sugars, amino acids (AAs) and monoamines within pulps using AuNP-assisted LDI-MSI for the first time, revealing that AAs and monoamines exclusively accumulated in the middle region near the seed zone. Monosaccharides and di/trisaccharides were generally distributed across entire pulps but exhibited different accumulation patterns. These findings provide a guide for breeding new varieties and improving extraction efficiency of bioactive compounds.

1. Introduction

As one of the most important and popular tropical fruits worldwide, banana (*Musa* spp.) is widely accepted by consumers due to its high nutritional value (Qamar & Shaikh, 2018; Singh et al., 2016; Yun et al., 2022), and has gained attention for its antioxidant and antimicrobial capacity attributed to ubiquitous polyamines and bioactive amines (Adão & Glória, 2005; Lima et al., 2008). Among these compounds, dopamine and noradrenaline afforded a higher antioxidant capacity than other natural antioxidants (Borges et al., 2019), which have significant potential to contribute to the development of pharmaceutical formulations for some disease treatment (Breitel et al., 2021; Mondal et al., 2021; Pereira & Maraschin, 2015). In addition to bioactive amines, banana pulp also provides plenty of valuable nutraceuticals and bioactive compounds, such as carbohydrates, amino acids (AAs), carotenoids, polyphenols, and phytosterols (Maduwanthi & Marapana, 2021; Mondal et al., 2021; Sidhu & Zafar, 2018; Singh et al., 2016). Given that the nutritional quality of bananas depends on the metabolic changes occurring during development and postharvest senescence, a systematic investigation of the dynamic alteration in metabolite profiles of banana pulp has been highly desired.

There exist significant physicochemical and biochemical changes in various metabolites occur during ripening of banana fruits (Valérie Passo Tsamo et al., 2014). Conventional liquid chromatography mass spectrometry (LC-MS) and gas chromatography MS (GC–MS) has proven to be a robust tool for the detection of nonvolatile (Adão & Glória, 2005) and volatile metabolites (Boudhrioua et al., 2003), respectively, in banana peels and pulps. Specifically, Adão *et al.* demonstrated that the contents of starch, soluble sugars, and bioactive amines vary with each individual during the ripening of 'Prata' banana using LC-MS analysis (Adão & Glória, 2005). Borges *et al.,* revealed that the levels of various bioactive amines, including tyramine, histamine, dopamine, serotonin,

* Corresponding authors.
E-mail addresses: yiganjun@gdaas.cn (G. Yi), shijuan@agrogene.ac.cn (S. Yan).
[1] These authors contributed equally to this work.

https://doi.org/10.1016/j.fochx.2022.100371
Received 27 April 2022; Received in revised form 1 June 2022; Accepted 15 June 2022
Available online 20 June 2022

spermidine, and spermine decreased in the pulps during fruit ripening processes (Borges et al., 2019). Alteration in levels and retention of provitamin A carotenoids during ripening of eight banana varieties have also been previously reported (Ekesa et al., 2015). Recently, to investigate how lipid accumulation is regulated during banana ripening, Sun *et al.* generated a comprehensive atlas of lipidomic changes in *Musa cavendish* using targeted lipidomics (Sun et al., 2020). Using a different approach, nuclear magnetic resonance (NMR)-based metabolomics analysis, Yuan *et al.,* revealed alterations in primary and secondary metabolites (e.g., AAs, carbohydrates, and phenolics) in banana fruits during postharvest senescence (Yuan et al., 2017). Unfortunately, the masking of stochastic average values by pulp homogenates and the resultant loss of spatial information in both MS- or NMR-based holistic metabolomics studies have hindered their further development.

To circumvent these issues, MS imaging (MSI) techniques have been used as a label-free and non-specific detection tool to provide the spatiotemporal distribution information on a broad range of metabolites in biological tissues (Li et al., 2021; Yin et al., 2019). In recent years, several efforts have been made to develop matrix-assisted laser desorption/ionization (MALDI)-MSI technologies for mapping metabolite abundances in various fruits and vegetables, such as strawberry and apple fruits (Horikawa et al., 2019), soybean root nodules (Samarah et al., 2021), and tomato fruits (Dong et al., 2020). In addition, Hölscher *et al.* used ^{1}H NMR spectroscopy, laser desorption/ionization (LDI)-MSI, and Raman spectroscopy to identify and locate phenylphenalenones, a banana-specific type of phytoalexins, within the *Musa* spp. epidermis and roots infected by *Radopholus similis* (Hölscher et al., 2014). Recently, Wu et al. have proposed a gold nanoparticle (AuNP)-immersed paper imprinting MSI strategy for visualizing the spatial distribution of some endogenous compounds within banana corms (Wu et al., 2020). Despite these efforts, there are few studies in the literature reporting the unique spatiotemporal distribution of bioactive compounds within banana pulps, especially for different post-ripening stages. Meanwhile, the limited molecular coverage and quantitative capability of MSI still render it challenging to discover key differentially abundant and spatially distinct patterns of metabolites. To overcome these limitations, spatially resolved metabolomics, which was developed by integrating optimized MSI and metabolomics methods, has been proposed for the accurate determination of compositions, contents, and spatial distribution of endogenous and exogenous metabolites in biological tissues and single cells (Pareek et al., 2020; Sun et al., 2019). However, its potential for the investigation of alterations in metabolite contents and spatial patterns within banana pulps during postharvest senescence has yet to be explored.

Here, we used integrated AuNP-assisted LDI-MSI and GC–MS-based metabolomics to compare the levels and spatiotemporal distribution of various metabolites within banana pulps between the Brazil and Dongguan varieties during the first 8-days of postharvest ripening. The combined results collectively suggest that there are higher levels of most AAs and monoamines in Brazil banana pulps than in Dongguan pulps, and the levels of individual compounds varied to a large extent as a function of post-ripening time. Moreover, AAs and monoamines were found to be co-localized with a tissue-specific distribution pattern accumulating in the middle region near the seed zone of banana pulps. Although mono-, di- and trisaccharides ubiquitously distributed in the whole pulp, the monosaccarides exhibited different accumulation patterns from the higher-order sugars.

2. Materials and methods

2.1. Chemicals and materials

Chloroauric acid ($HAuCl_4$, ≥99.9% purity), sodium citrate (99% purity), gelatin from porcine skin, α-cyano-4-hydroxycinnamic acid (CHCA), 2,5-dihydroxybenzoic acid (DHB), D-(+)-xylose (99% purity), D-(+)-glucose (≥99.5% purity), sucrose (99% purity), D-(+)-raffinose pentahydrate (≥98% purity), γ-aminobutyric acid (GABA, ≥99% purity), L-serine (≥99% purity), L-alanine (≥98% purity), glycine (≥99% purity), L-proline (≥99% purity), L-valine (≥98% purity), L-threonine (≥98% purity), L-leucine (≥98% purity), L-proline (≥99% purity), L-lysine (≥98% purity), L-methionine (≥98% purity), L-phenylalanine (≥98% purity), L-histidine (≥99% purity), L-arginine (≥98% purity), L-tyrosine (≥98% purity), L-tryptophan (≥98% purity), methyl *tert*-butyl ether (MTBE), and *N*-methyl-*N*-(trimethylsilyl) trifluoroacetamide (≥98.5% purity) were purchased from Sigma Aldrich (St. Louis, MO, USA). Conductive indium tin oxide (ITO) coated glass slides were obtained from Bruker (Bremen, Germany).

2.2. Banana materials

Two typical banana varieties, Brazil banana (*Musa* spp., AAA) and Dongguan banana (*Musa* spp., ABB), were selected for this study. The fruits of both varieties at different stages, namely 1 day, 2 days, 3 days, 4 days, 5 days, 6 days, 7 days, and 8 days after postharvest treatment with ethylene to initiate ripening, were collected from the field of National Musa collections in Guangzhou, Guandong province, China. The pulp of fruits was separated from the peel, and cut into several slices, frozen in liquid nitrogen immediately, then stored at − 80 ℃ for further metabolomic and MSI analysis. Six biological replicates were collected for each banana genotype.

2.3. Preparation of MALDI matrices, standard mixtures, and gold nanoparticles

The MALDI matrices, DHB and CHCA, were dissolved in 70/30 (v/v) water/acetonitrile with 0.1% trifluoroacetate. And 10 mg/mL DHB and CHCA were adopted as the final concentration for LDI-MS experiments. All the analytes, including D-(+)-xylose, D-(+)-glucose, sucrose, D-(+)-raffinose pentahydrate, GABA, L-serine, L-alanine, glycine, L-proline, L-valine, L-threonine, L-leucine, L-proline, L-lysine, L-methionine, L-phenylalanine, L-histidine, L-arginine, L-tyrosine, and L-tryptophan, were dissolved in water/methanol (1:1, v/v) at a concentration of 10 mM. All stock solutions were kept at 4 ℃ before use. Mixed solutions of AAs and sugars were then prepared by mixing and diluting stock solutions to a final concentration of 1 mM for each analyte, respectively. Synthesis of the AuNP solution was performed according to the previous reports (Qin et al., 2021; Wu et al., 2020). Briefly, 1 g chloroauric acid ($HAuCl_4$) was dissolved in 50 mL H_2O as the stock solution. Then, 1 mL stock solution was diluted to 100 mL for preparing the $HAuCl_4$ solution at a concentration of 0.1 mg/mL. This $HAuCl_4$ suspension was heated to boiling and quickly mixed with 2 mL 10 mg/mL sodium citrate with high-speed stirring. After refluxing at a constant temperature for 10 min, the solution was cooled to room temperature and stirred for 15 min. Finally, the as-prepared AuNP suspensions were ready for matrix spraying. In the AuNP-assisted LDI-MS analysis, 1 μL droplet of 0.1 mg/mL AuNP suspension in aqueous solution and 1 μL droplet of 1 mM AA mixture solution or sugar mixture solution were first mixed and then deposited on the surface of commercial stainless steel plate. A total of 2 μL volume of mixture solution was spotted for MS analysis.

2.4. Metabolomics analysis using GC–MS

Freeze-dried banana pulp samples were used for metabolomics analysis with six biological replicates for each sample. Fifty micrograms of banana pulp powder from each sample was extracted following the procedures described in a previous study (Heng et al., 2019). Briefly, banana pulps of two varieties were ground to powder under liquid nitrogen, and extracted ultrasonically with 1 mL pre-cooled extraction solvent (MTBE, 3:1) at − 20 °C for 5 min at 4 °C. Extracts were centrifuged at 23,128 *g* at 4 ℃ for 10 min. For phase separation, a volume of 500 μL of mixture solvent (methanol/water = 1/3) was added to each tube and the samples were vortexed thoroughly for 1 min. Finally, a

fixed volume of 200 μL of the polar phase (located at the lower phase) after centrifugation was transferred into a 1.5 mL centrifuge tube that was dried in a SpeedVac concentrator without heating. A dried 150 μL aliquot from the polar phase was derivatized with *N*-methyl-*N*-(trimethylsilyl) trifluoroacetamide for primary metabolite profiling and then analyzed using GC–MS (7890A-5975C, Agilent, USA) as described previously (Chen et al., 2022). Quality control (QC) samples, in which small aliquots of each biological sample to be studied were pooled and thoroughly mixed, were embedded in the batch every 10 test samples during the GC–MS analysis to assess the performance of the system and also used for normalization as described previously (Dunn et al., 2011). GC–MS raw data were firstly evaluated and deconvoluted using MassHunter Qualitative Analysis B.06.00 software (Agilent Technologies Inc., Santa Clara, CA, USA). Then the peak integration and alignment were processed using MassHunter Quantitative Analysis B.07.01 software (Agilent Technologies Inc., Santa Clara, CA, USA). Finally, the NIST mass spectral library and an in-house mass spectral database established using authentic standards were used together for metabolite identification (Yan et al., 2021). Their retention indices were compared with *n*-alkanes ranging from C7-C36 for identification of volatile and non-volatile silylated metabolites according to previous reports (Table S1) (Baky et al., 2022). Based on the normalized metabolomic data, the heat maps of detected metabolites was drawn using TBtools (v1.082, Guangzhou, China). In addition, multivariate statistical analyses were then performed using SIMCA software version 13.0.3 (Umetrics, Umea, Sweden), including principal component analysis (PCA), orthogonal projections to latent structures discriminant analysis (OPLS-DA), hierarchical cluster analysis (HCA), and one-way analysis of variance (ANOVA).

2.5. MSI analysis using MALDI-TOFMS

All banana pulps used for MSI analysis were processed in the same batch as those for used metabolomics. Of particular note, because the intact banana pulps were too large for analysis, a representative triangular domain including the outer and center portions of flesh was cut for subsequent freezing sectioning and MSI analysis (red dotted box in Fig. S1). Each banana slice with different varieties and postripening stages used for MSI analysis was taken from the middle position of whole banana pulps. Briefly, banana pulps were first snap-frozen in liquid nitrogen and uniformly embedded with gelatin, which comes to a temperature equilibrium in the freezing microtome (HM560, Leica Microsystems Inc., Wetzlar, Germany) for 20 min. Then, banana pulps were sectioned to a 25 μm thickness at − 20 ℃ and thaw-mounted onto ITO-coated glass slides (Bremen, Germany). The slides were placed in a vacuum desiccator for 30 min to remove the excess water content. Finally, the as-prepared AuNP matrix was sprayed uniformly using a high-performance ultrasonic sprayer (UAM4000, Hangzhou, China). Details of the spraying parameters can be found in Table S2. In this study, sodium citrate was adopted as the reducing agent and dispersant agent for the preparation and use of AuNP suspension to avoid excess background interferences and self-aggregation. Before spraying, the AuNP suspension was fully dispersed with ultrasound assistance so that the spraying process can be sustained for a relatively long time regardless of self-aggregation of AuNPs.

All MSI measurements were performed on a MALDI time-of-flight (TOF) mass spectrometer (UltrafleXtreme, Bruker Daltonics, Bremen, Germany) instrument equipped with a 355 nm Nd: YAG laser and 1,000 Hz repetition rate. MS calibration was accomplished using gold cluster ions (Au_n^+) derived from AuNPs due to their simple isotope patterns, including Au^+ (*m/z* 196.966), Au_2^+ (*m/z* 393.932), Au_3^+ (*m/z* 590.899), Au_4^+ (*m/z* 787.866), and Au_5^+ (*m/z* 984.832). Considering that banana pulps have the relatively large area, a “small” laser spot and a pixel size of ~ 80 μm were used to acquire the satisfactory acquisition time and imaging resolution, respectively. Mass spectra were acquired in the positive ion reflection mode with a mass range from 100 to 1,000 Da. Unless otherwise indicated, the mass spectrum at each pixel was averaged across 200 laser shots. The laser energy was set at 85% for MSI experiments. The detailed parameters for the MS analysis were as follows: 20.00 kV for the ion source voltage, 11.00 kV for the lens voltage, and 20.84 kV for the reflector voltage. MSI data were processed using flexAnalysis 3.4 (Bruker Daltonics, Bremen, Germany) and flexImaging 2.1 (Bruker Daltonics, Bremen, Germany).

3. Results

3.1. Metabolite profiling of Dongguan and Brazil banana pulps during postharvest senescence

To investigate the global metabolic differences between Dongguan and Brazil banana pulps during the 8-day postharvest ripening stages, GC–MS-based metabolomics analysis was performed. A total of 116 metabolites were detected in the banana pulp samples (Table S1 and Fig. S2). Among them, 65 metabolites were conclusively identified based on an in-house mass spectral database established using authentic standards, including 22 AAs, 12 sugars and sugar alcohols, 14 organic acids, seven tricarboxylic acid cycle (TCA)-related metabolites, four monoamines, and six other compounds (Fig. 1A). AA and sugar metabolism-related metabolites constituted the largest class of identified metabolites, representing about 35.38% and 21.54% proportion of identified compound numbers among the total components, respectively. Furthermore, PCA was applied to examine intrinsic variation in the banana dataset (Fig. S3), and then OPLS-DA model was conducted to enhance the separation between the groups (Fig. 1B, Table S3). The OPLS-DA model performance for both Dongguan banana dataset and Brazil banana dataset was evaluated using permutation test repeated 200 times (Fig. S4). As shown in Fig. 1B, the metabolome data of both Dongguan and Brazil banana pulps at different postharvest days could be clearly distinguished except for 1-day and 2-day Dongguan banana samples, suggesting that large metabolic differences exist between each postharvest ripening stage. The 1-day, 2-day, and 3-day samples from the Brazil banana variety were relatively dispersed, which indicated that the metabolic change during the early postharvest stages in Brazil banana pulps occurred faster than that in Dongguan banana pulps.

3.2. Differential metabolites in Brazil and Dongguan banana pulps during postharvest senescence

To further summarize the overall metabolic changes in Dongguan and Brazil banana pulps during ripening, heatmap analysis was performed. The heatmap revealed changes in the relative levels of various metabolites, including sugars and sugar alcohols, AAs, monoamines, and organic acids (Fig. 2 and Table S4). The levels of most soluble sugars, such as glucose, fructose, sucrose, and raffinose, increased significantly as a function of time for both banana pulps. In sharp contrast, glycerol-3-phosphate (Gly3P) and glucose-6-phosphate (G6P) levels decreased with time. Interestingly, although the levels of most soluble sugars were quite comparable, the contents of some sugar metabolism-related metabolites, namely *meso*-erythritol, arabitol, mannitol, myo-inositol, and galactose, were higher in Dongguan banana pulps than in Brazil pulps. Higher levels of most AAs accumulated in the Brazil variety than the Dongguan sample. Notably, the levels of valine, leucine, isoleucine, glycine, serine, alanine, GABA, and tyrosine in Brazil banana pulps increased during the 8 days of postharvest ripening stages, while the levels of aspartic acid, arginine, glutamine, phenylalanine, histidine, and methionine gradually decreased.

In addition, the contents of some monoamine metabolism-related metabolites, such as norepinephrine, were higher in the pulp of Brazil banana than in that of Dongguan banana, suggesting that the activation of the monoamine metabolic pathway during postharvest ripening was variety dependent. Of particular note, the levels of tyrosine and norepinephrine in Brazil banana pulp increased as a function of time,

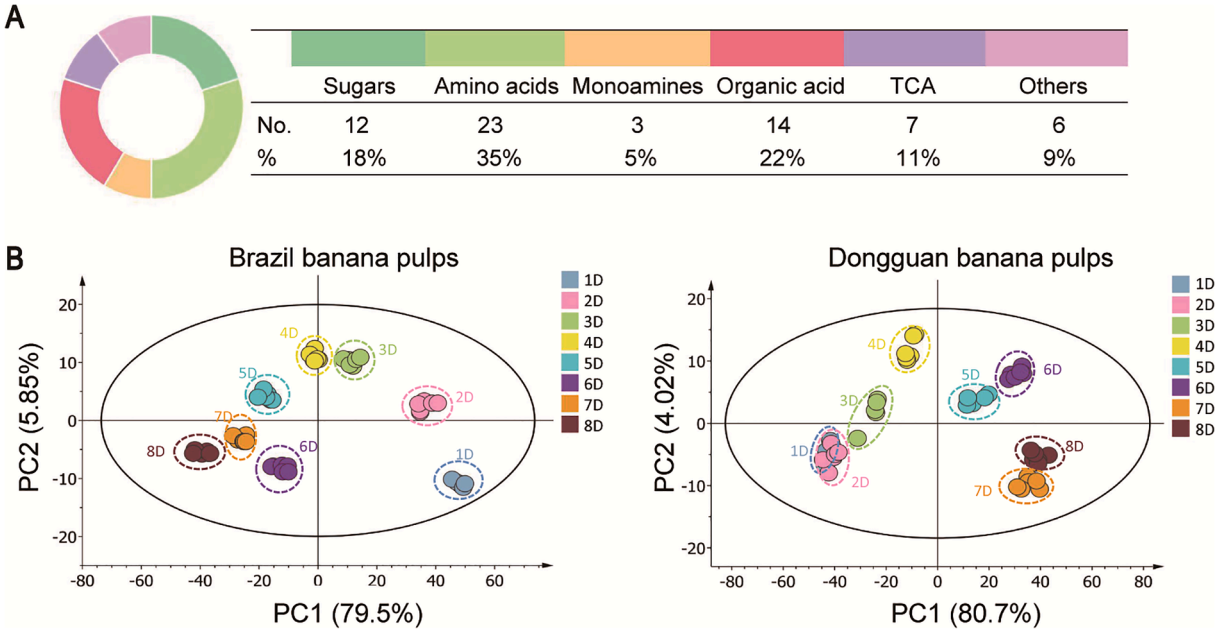

Fig. 1. (A) The classification and proportion of identified metabolites in banana pulps obtained using GC–MS, including sugars and sugar alcohols, amino acids, monoamines, organic acids, TCA intermediates. (B) OPLS-DA score plots of GC–MS data for Brazil banana and Dongguan banana samples from different postharvest ripening stages.

whereas the levels of tyramine and dopamine increased until 3 days postharvest ripening and then a significantly decreased when the pulp became overripe. In sharp contrast, the content of dopamine gradually increased in Dongguan banana pulps beginning at 3 days postharvest. In addition, the levels of several organic acids including glyceric acid, pipecolic acid, ferulic acid, and linoleic acid gradually decreased, whereas nicotinic acid, gluconic acid, and uric acid levels promoted as the ripening time increased for Brazil banana fruits. However, pyruvic acid, oxalacetic acid, citric acid, and malic acid in Dongguan banana pulps first increased and then decreased. Taken together, the results presented here indicate that these functional metabolites differed not only between different postharvest ripening stages but also between banana varieties.

3.3. *Improved sensitivity of metabolite detection in banana pulp using AuNP-assisted LDI-MS*

MALDI has several inherent disadvantages due to the use of organic matrices, such as severe background interference in low mass region (m/z < 500 Da), which hinders chemical identification of small-molecule metabolites, and limited ionization efficiency of small molecules in some cases, especially for neutral AAs and carbohydrates (Wang et al., 2020). To improve the molecular coverage and detection sensitivity of functional metabolites in banana pulps, a comparison between conventional MALDI matrices (e.g., CHCA and DHB) and AuNPs for 16 AAs and four soluble sugars were investigated, respectively (Fig. 3 and Fig. S5). As shown in Fig. 3B-C, only nine AAs were detected with relatively low signal-to-noise ratio (SNR) using either CHCA or DHB due to low protonation efficiency and strong background interferences in the low m/z range. In contrast, all 16 AAs were detected with a high SNR using AuNP-assisted LDI-MS (Fig. 3A). In particular, the results revealed that most AA molecules can be detected as the ion forms of protonated, sodium or potassium adducts, suggesting that AuNPs could improve the ionization efficiency of AAs that were not prone to protonation. Moreover, because ripened banana is also rich in soluble sugars in addition to AAs, further proof-of-concept tests for AuNP-assisted LDI-MS detection were evaluated using a mixed standard solution of oligosaccharides, including xylose, glucose, sucrose, and raffinose (Fig. S5). Interestingly, all the sugar molecules could be detected with high SNRs using AuNP-assisted LDI-MS. In contrast, xylose was hard to be detected because of the strong background interference generated from the CHCA and DHB matrices. Taken together, AuNPs have great potential for MSI analysis of AAs and oligosaccharides in banana pulp because they show improved desorption/ionization efficiency and less spectral interferences.

3.4. *Spatial differentiation of soluble sugars in Dongguan and Brazil banana pulps during postharvest ripening*

We used AuNP-assisted LDI-MSI for mapping the spatial distribution and temporal accumulation processes of a broad range of metabolites within banana pulps. Fig. 4A displays the schematic workflow of AuNP-assisted LDI-MSI for banana pulps, including freezing sectioning, AuNP solution deposition, and pixel-by-pixel laser sampling. The dynamic spatiotemporal location of three soluble sugars (i.e., monosaccharides, disaccharides, and trisaccharides) within Dongguan and Brazil banana pulps, ranging from 1 day to 8 day after postharvest senescence, can be clearly seen in Fig. 4B-C. For the first two days of postharvest ripening, the content of monosaccharides and disaccharides were relatively low, and trisaccharides were barely detected in Dongguan banana pulps in the initial ripening period. Similarly, that the contents of the three kinds of soluble sugars in Brazil banana pulps were too low to visualize. In contrast, the contents of the three kinds of soluble sugars, especially monosaccharides and disaccharides, in both varieties increased beginning at 3 days postharvest, and the levels were highest from days 6 to 7. This can be explained by an increase in the rate of amylohydrolysis, which was in accordance with the GC–MS quantification results of monosaccharides and disaccharides (Fig. 2). Of particular note, the three kinds of soluble sugars were not distributed evenly within the banana pulp. Monosaccharides were abundant in the intermediate micro-region for both banana varieties, while disaccharide and trisaccharide levels were higher in the whole pulps rather than the micro-region where monosaccharides accumulated.

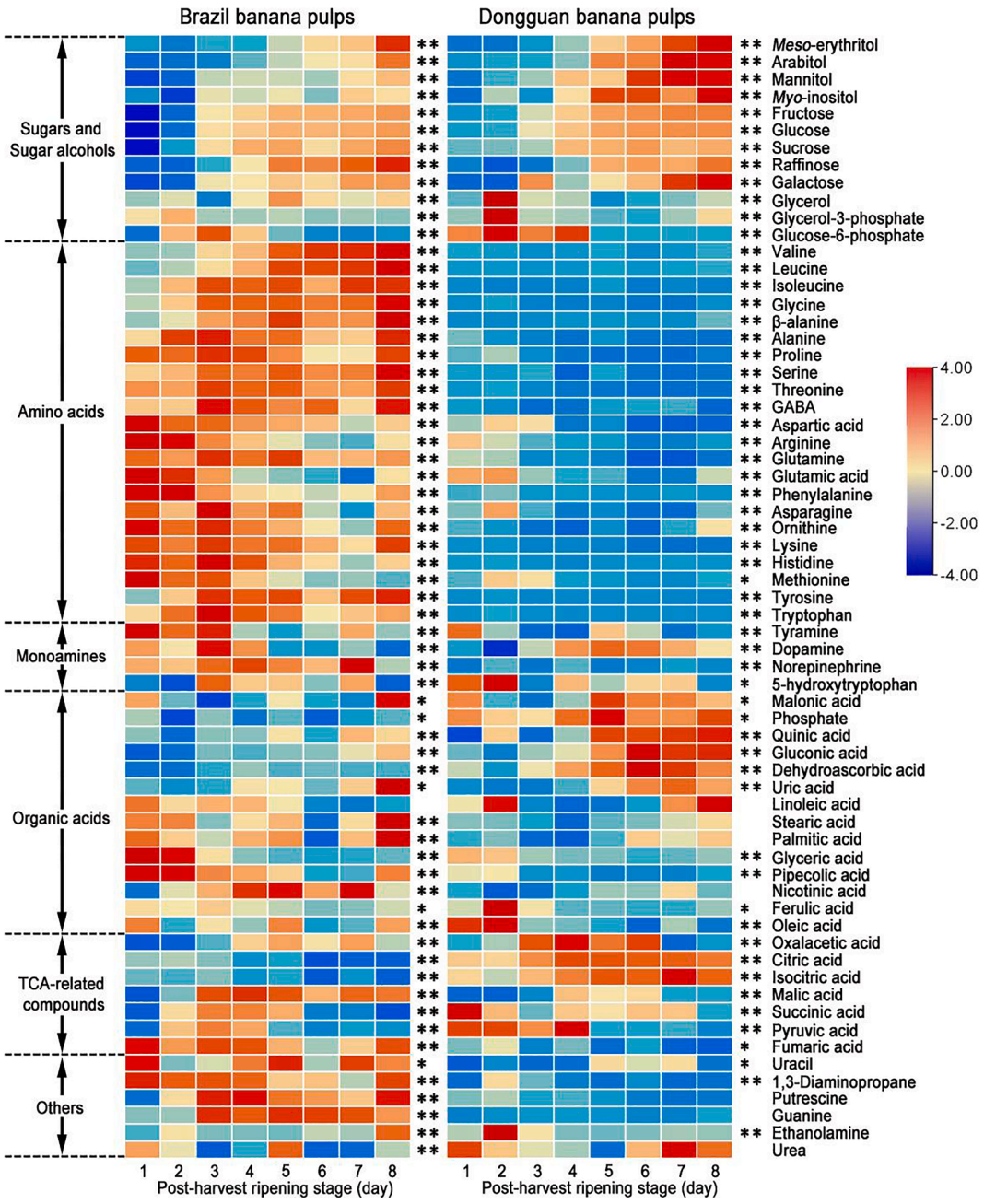

Fig. 2. Heatmaps of 65 identified metabolites in banana pulp showing the differences in Brazil and Dongguan banana varieties during 8 days postharvest ripening stages. The red color indicates a higher level of the detected metabolites using GC–MS, whereas the blue color indicates a lower level of them. "*" and "**" correspond to sample groups with significant differences of $0.01 \leq p\text{-value} \leq 0.05$ and $p\text{-value} \leq 0.01$ using ANOVA, respectively.

3.5. Spatial differentiation of AAs and monoamines in Dongguan and Brazil banana pulps during postharvest ripening

In addition to determining the distribution of sugars, we further visualized the spatiotemporal distribution of a selected subset of functional AAs, such as threonine, glutamine, and arginine. As shown in Fig. 5, AAs were detected with high SNRs within Dongguan and Brazil banana pulps, but the arginine content was hard to detect within Dongguan banana pulps beginning at 6 days postharvest using MSI, which is probably because the content of arginine is lower in Dongguan banana than in the Brazil variety. In addition, the tissue-specific distribution patterns of AAs were more obvious compared with those of soluble sugars. Specifically, all three AAs almost exclusively accumulated in the middle region near the seed zone. The spatiotemporal distribution of asparagine and histidine were also obtained (Fig. S6), indicating that these two AAs had a distribution patterns similar to those of the other AAs. And their contents were relatively lower in Dongguan banana pulps than in Brazil banana pulps, which is in agreement with the previous GC–MS results (Fig. 2). To better understand the basic roles of monoamines that accumulate within different micro-regions of banana pulp, we further visualized the differential distribution of monoamines in Dongguan and Brazil banana using AuNP-assisted LDI-MSI. Inspection of the images (Fig. S7) revealed that dopamine, L-DOPA, and noradrenaline were almost completely co-localized and were mainly located in the middle region near the seed zone, exhibiting distribution patterns similar to those of AAs.

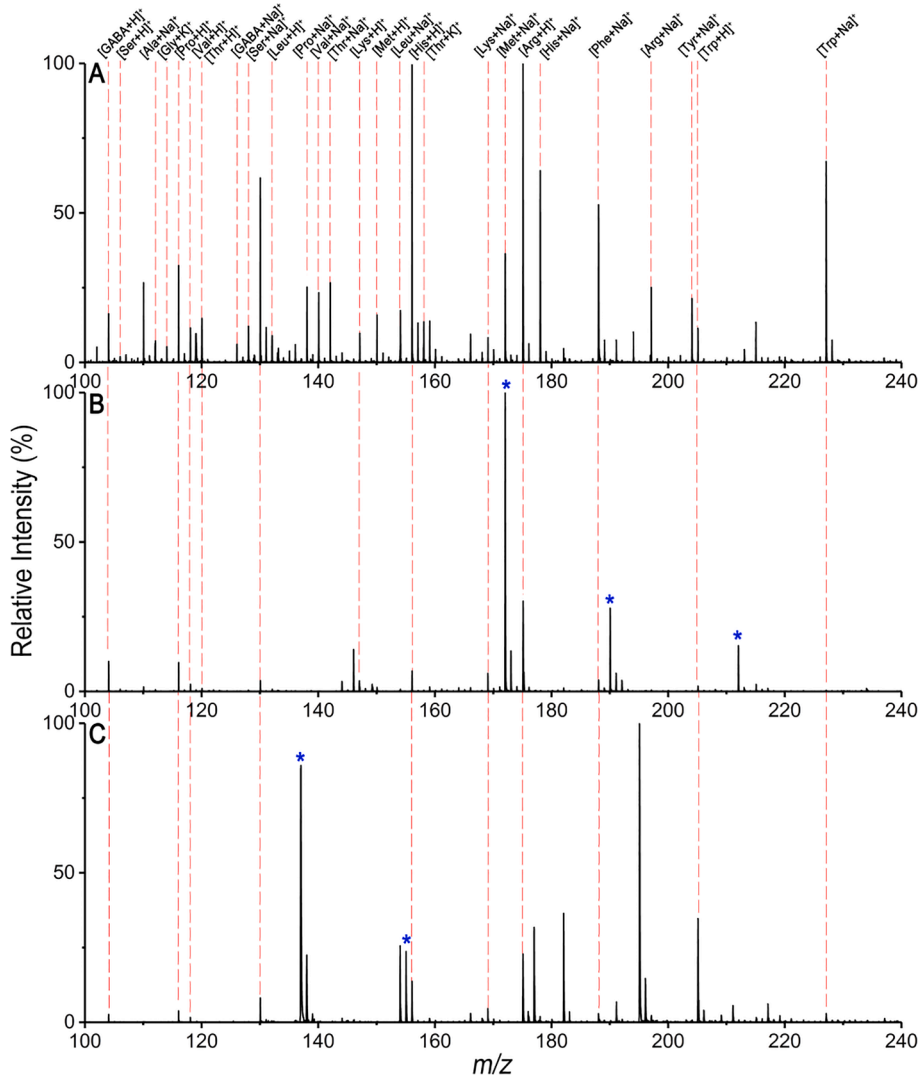

Fig. 3. Comparative LDI mass spectra of 16 amino acid mixtures obtained using (A) AuNPs, (B) CHCA, and (C) DHB matrices. The concentration of each analyte is 1 mM. *denotes the background peaks derived from conventional matrices.

4. Discussion

The onset of the ripening of banana pulps is accompanied by intricate and irreversible metabolic changes, such as degradation of chlorophyll, conversion of starch into soluble sugars, and accumulation of functional metabolites, which result in peel color change, pulp softening and sweetening, as well as development of characteristic aroma, respectively (Guo et al., 2018; Nascimento et al., 2019; Xiao et al., 2021). Thus, the development of quality attributes in bananas can be significantly affected by the levels and spatiotemporal distribution of these functionally bioactive compounds across the post-ripening period. In the present study, we investigated the levels and spatiotemporal distribution of various functional metabolites within the pulps of two banana varieties (i.e., Brazil and Dongguan) during postharvest senescence. The targeted metabolomics results indicated that the levels of most soluble sugars increased significantly as a function of time for both banana varieties. Moreover, higher levels of most AAs and monoamines can be observed in the Brazil banana pulp than in the Dongguan banana pulp. In addition, the spatiotemporal distribution of metabolites in both banana varieties was also visualized for the first time using AuNP-assisted LDI-MSI. Of particular note, although three soluble sugars were found to ubiquitously distribute across the whole banana pulp, monosaccharides display a different accumulation pattern from disaccharides and trisaccharides. Meanwhile, AAs and monoamines were found to almost exclusively accumulate in the middle region near the seed zone. Therefore, this spatially resolved metabolomics method allows for visualization of a spatial metabolic network closely related to the ripening process of banana fruit pulps at the metabolic level, providing a guide for breeding new varieties and improving the extraction efficiency of bioactive compounds.

4.1. High amino acid and monoamine levels are correlated with banana pulp varieties and postharvest ripening stages

AAs are important nutrients in banana fruits, and their metabolism frequently occurs during postharvest senescence. Our metabolomics results indicated that the levels of most AAs were higher in Brazil banana pulps than in Dongguan banana pulps, and the levels of the individual compounds as a function of post-ripening time varied to a large extent in Brazil banana pulps. Specifically, we found that the levels of amino acids derived from the glycolytic pathway, including valine, leucine, isoleucine, glycine, serine, alanine, GABA, and tyrosine, significantly increased during the postharvest ripening process. In sharp contrast, the levels of TCA cycle-derived amino acids, including aspartic acid, arginine, glutamine, phenylalanine, histidine, and methionine, gradually decreased during the postharvest ripening process. This unique content

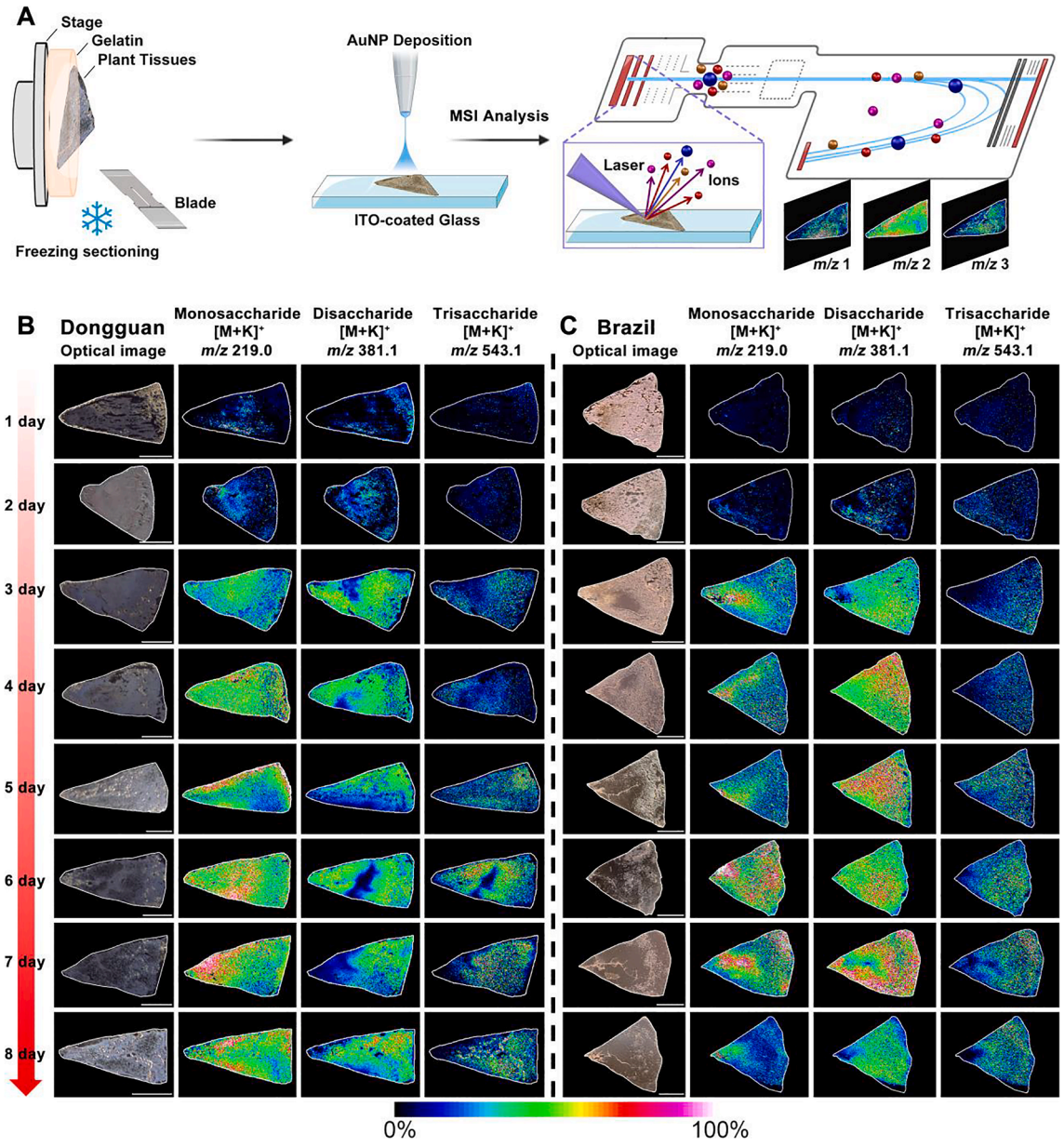

Fig. 4. (A) Schematic workflow of AuNP-assisted LDI-MSI for banana pulps, including freezing sectioning, AuNP solution deposition, and pixel-by-pixel laser sampling. Part of the schematic workflow was created using BioRender (https://biorender.com/). The dynamic spatial distribution of monosaccharides ($[M + K]^+$, *m/z* 219.0), disaccharides ($[M + K]^+$, *m/z* 381.1), and trisaccharides ($[M + K]^+$, *m/z* 543.1) within (B) Dongguan banana pulps and (C) Brazil banana pulps during postharvest senescence from day 1 to day 8. Scale bars, 5 mm.

alteration of various amino acids might be explained that postharvest ripening stages could contribute to high rates of the glycolysis pathway and the TCA cycle. Our results and previous studies have revealed that sugar levels of banana fruits can be significantly enhanced along with postharvest days (Adão & Glória, 2005; Boudhrioua et al., 2003; Campuzano et al., 2018; Yuan et al., 2017). Given sugars are the initial precursors of most amino acids derived from the glycolytic pathway, higher contents of sugars as a function of postharvest ripening stages contribute to the levels of most glycolysis-derived amino acids. In sharp contrast, TCA cycle can be remarkably promoted during postharvest ripening stages, resulting in the relatively low level of TCA cycle-derived amino acids.

In addition to AA synthesis, decarboxylation of AAs or amination of aldehydes and ketones can contribute to the formation of bioactive amines. Thus, banana pulps or peels also exhibit a high content of various bioactive amines (e.g., serotonin, dopamine, and norepinephrine), and the levels of these amines can be dependent upon the banana variety (Singh et al., 2016). Several studies have revealed that the ubiquitous polyamines and bioactive amines within banana pulps are closely associated with antioxidant activity but their contents vary in different varieties and postharvest ripening stages (Adão & Glória, 2005; Lima et al., 2008). These findings are in agreement with our observation using GC–MS-based metabolomics that the levels of most monoamines were higher in Brazil banana pulps than in Dongguan pulps (Fig. 2). In addition, we found that the contents of most monoamines (e.g., tyramine, dopamine, and norepinephrine) in Brazil banana pulps decreased during postharvest senescence. These results were consistent with the finding of a recent study that the levels of various bioactive amines, including tyramine, histamine, dopamine, serotonin, spermidine, and spermine, decrease in the pulp during fruit ripening processes (Borges et al., 2019). Given that tyramine is closely associated with allergenic and intoxication processes, deeper insights into the

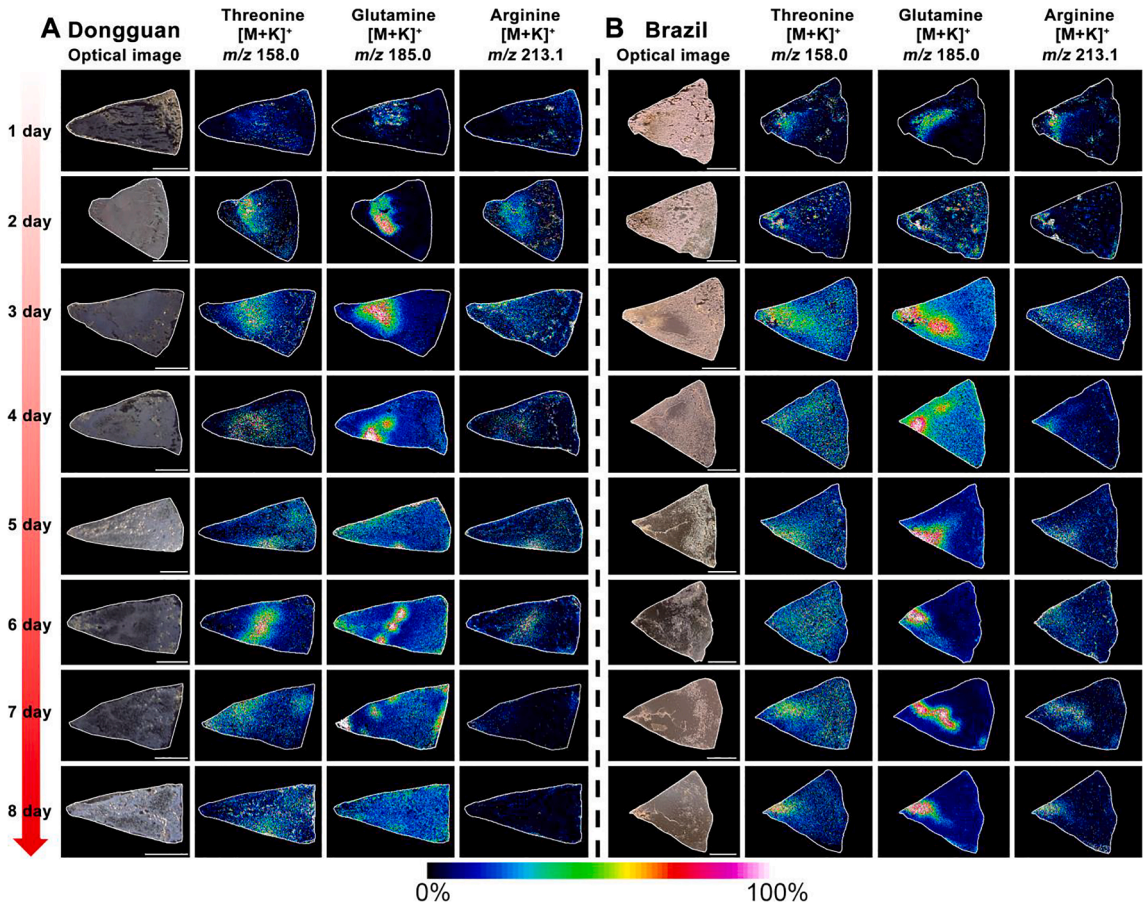

Fig. 5. The dynamic spatial distribution of threonine ($[M + K]^+$, *m/z* 158.0), glutamine ($[M + K]^+$, *m/z* 185.0), and arginine ($[M + K]^+$, *m/z* 213.1) within (A) Dongguan banana pulps and (B) Brazil banana pulps during postharvest senescences from day 1 to day 8. Monamines were consistently detected as a form of potassium adduct $[M + K]^+$ due to their high contents within banana pulps. Scale bars, 5 mm.

differential expression of these monoamines during ripening of different banana varieties is of vital importance for quality evaluation in food (Singh et al., 2016). In contrast, the content of dopamine in Dongguan banana pulps was found to increase along with the number of postripening days, and the content was the highest point ranging from days 5 to 6. Considering that banana species have proven to be a good resource for the extraction of dopamine and its precursors, which can be developed as a promising pharmaceutical formulation for Parkinson's disease treatment (Pereira & Maraschin, 2015), their metabolic profiles as a function of postharvest stages could prompt for further studies on extraction and utilization of bioactive compounds. Taken together, the results presented here suggest that the levels and dynamic variations in AAs and bioactive monoamine levels are not only affected by the postharvest ripening stage but also the variety of banana.

4.2. Tissue-specific accumulation of amino acids, and monoamines in the middle region near the seed zone.

To date, the alteration of metabolite levels during the postharvest stage of banana fruits has been widely investigated using targeted and untargeted metabolomics (Adão & Glória, 2005; Borges et al., 2019; Boudhrioua et al., 2003; Campuzano et al., 2018; Maduwanthi & Marapana, 2021; Sun et al., 2020; Yuan et al., 2017). However, the spatiotemporal distribution of these bioactive compounds within pulps has yet to be fully addressed. In the present study, we systematically investigated the spatiotemporal distribution of soluble sugars, AAs, and monoamines among different banana variants and postharvest ripening stages using MSI for the first time. Our targeted metabolomics results indicated that the levels of most soluble sugars increased significantly as a function of time for both banana varieties except for Gly3P and G6P, which decreased along with the postharvest time (Fig. 2). This was in accordance with previous reports and our MSI data (Fig. 4B-C) that accumulation of sugars due to the degradation of starch occurred during fruit ripening processes (Borges et al., 2019; Marriott & Palmer, 1980; Yap et al., 2017). Fruit sweetness is one of the major factors in evaluating fruit quality, which can be decided by the contents and locations of monosaccharides (e.g., glucose and fructose) and disaccharides (e.g., sucrose). These sugar species play a crucial role in the development and maturation processes of fruits, promoting the yield and quality of banana pulps. Interestingly, the MSI results revealed that three types of soluble sugars were not distributed evenly within the banana pulp. Of note here is the fact that monosaccharide and disaccharide exhibited the different accumulation patterns based on MSI results, suggesting that hydrolysis rate of soluble disaccharides to monosaccharides might be microregion-dependent in banana pulps. The hydrolysis rate is observed to be remarkably expedited in the middle region near the seed zone where the contents of monosaccharides and disaccharides were elevated and decreased, respectively. This phenomenon is similar to the tissue-specific accumulation patterns of AAs and bioactive amines. Thus, it requires further validation in a future study to clearly illustrate the microregion-specific hydrolysis involved in banana pulps during the postharvest ripening stages.

Moreover, dopamine, L-DOPA, and noradrenaline displayed almost the same localization patterns as AAs and were mainly located in the middle region near the seed zone (Fig. S7). Previous studies have reported that compared with whole banana pulps, the seed region has significantly higher antioxidant activity (Qamar & Shaikh, 2018), which is consistent with our MSI results. Given that biologically active amines

afford many health-promoting and disease-preventing effects, pinpointing their location within banana pulps facilitates the extraction and utilization of these bioactive compounds. Agudelo-Romero et al. reported that some monoamines, which are involved in the control and regulation of responses to biotic and abiotic stress, are closely associated with the quality and postharvest useful lifespan of the banana pulp (Agudelo-Romero et al., 2013). Among these monoamines, spermidine and spermine have been found to play a crucial role in cellular growth and division, as well as fruit senescence (Borges et al., 2019). Compared with conventional metabolomics analysis, the spatiotemporal visualization strategy used here might provide more insights into the biosynthesis and accumulation of various metabolites in banana pulps, leading to the improvement of the extraction of functional metabolites. Taken together, the integrated metabolomics and MSI results indicated that fine-tuned alterations and differential distribution in fruit metabolism during ripening contribute to the development of quality attributes in banana fruits.

Interestingly, we found that the bioactive compounds were consistently detected as a form of the potassium $[M + K]^+$ rather than the sodium $[M + Na]^+$ adducts using MSI, which might be due to the high contents of potassium within banana pulps (Aurore et al., 2009; Yap et al., 2017). In fact, several studies have revealed a strong positive correlation between potassium ion contents and the contents of total phenolics and non-structural carbohydrate (e.g., soluble sugars and starch), suggesting that potassium ions might contribute to carbohydrate translocation and the improved yield of total phenolics (Campuzano et al., 2018).

Despite their label-free and untargeted nature, MSI methods still suffer from limited chemical coverage and quantitative capability. Unlike homogenate extraction and chromatographic separation derived from LC–MS analyses, the desorption/ionization efficiency in laser-based sampling strongly depends on the matrix types, tissue-related matrix effects, and physicochemical properties of analytes (Wang et al., 2020). This explains why in most cases relative signal intensities obtained using MSI techniques do not represent the actual levels determined *via* LC–MS analyses. However, the overall trends in signal intensities of AAs in MS images agree with those acquired from banana extracts to a great extent. In addition, the chemical microenvironments of adjacent regions within the same tissue section can be chemically or morphologically different in some cases, resulting in varying matrix effects even within a single tissue section. Thus, further efforts are needed to achieve a higher detection sensitivity and a more precise quantification.

5. Conclusion

In summary, we demonstrated that the integration of AuNP-assisted LDI-MSI and untargeted metabolomics methods provides complementary information at the metabolic level, including how differential abundance and spatial distribution of metabolites within banana pulp variants at different stages of postharvest senescence. Specifically, metabolomics results demonstrated that both postharvest senescence and the banana variety can greatly influence the levels of AAs and monoamines. Moreover, MSI results revealed that the distribution of disaccharides within the banana pulp is co-localized as trisaccharides, whereas monosaccharides displayed a different accumulation pattern. Of particular note, Brazil banana pulps contains higher levels of most AAs and monoamines than Dongguan banana pulps, and these compounds were found to almost exclusively accumulate in the middle region near the seed zone. These results suggest that the development of quality attributes in bananas during postharvest senescence might be attributed to tissue-specific metabolic changes. Taken together, considering that monoamines (e.g., dopamine) have a strong antioxidant activity and anti-inflammatory effects, the ability to visualize the functional metabolites in pulps could provide a guide for breeding new varieties and improving the extraction efficiency of bioactive compounds.

Declaration of Competing Interest

The authors declare that they have no known competing financial interests or personal relationships that could have appeared to influence the work reported in this paper.

Acknowledgements

This work was jointly funded by the Key Realm R&D Program of Guangdong Province (No. 2020B0202090005), the Science and Technology Program of Guangdong Province (No.2021A0505030050), and the Special Fund for Scientific Innovation Strategy-Construction of High Level Academy of Agriculture Science (Nos. R2020PY-JX019 and R2021YJ-QG004). We would like to thank the Young Talent Support Project of Guangzhou Association for Science and Technology for support.

Appendix A. Supplementary data

Supplementary data to this article can be found online at https://doi.org/10.1016/j.fochx.2022.100371.

References

Adão, R. C., & Glória, M. B. A. (2005). Bioactive amines and carbohydrate changes during ripening of 'Prata' banana (*Musa acuminata*×*M. balbisiana*). *Food Chemistry, 90*(4), 705–711. https://doi.org/10.1016/j.foodchem.2004.05.020

Agudelo-Romero, P., Bortolloti, C., Pais, M. S., Tiburcio, A. F., & Fortes, A. M. (2013). Study of polyamines during grape ripening indicate an important role of polyamine catabolism. *Plant Physiology and Biochemistry, 67*, 105–119. https://doi.org/10.1016/j.plaphy.2013.02.024

Aurore, G., Parfait, B., & Fahrasmane, L. (2009). Bananas, raw materials for making processed food products. *Trends in Food Science & Technology, 20*(2), 78–91. https://doi.org/10.1016/j.tifs.2008.10.003

Baky, M. H., Shamma, S. N., Xiao, J., & Farag, M. A. (2022). Comparative aroma and nutrients profiling in six edible versus nonedible cruciferous vegetables using MS based metabolomics. *Food Chemistry, 383*, Article 132374. https://doi.org/10.1016/j.foodchem.2022.132374

Borges, C. V., Belin, M. A. F., Amorim, E. P., Minatel, I. O., Monteiro, G. C., Gomez Gomez, H. A., … Lima, G. P. P. (2019). Bioactive amines changes during the ripening and thermal processes of bananas and plantains. *Food Chemistry, 298*, Article 125020. https://doi.org/10.1016/j.foodchem.2019.125020

Boudhrioua, N., Giampaoli, P., & Bonazzi, C. (2003). Changes in aromatic components of banana during ripening and air-drying. *LWT - Food Science and Technology, 36*(6), 633–642. https://doi.org/10.1016/S0023-6438(03)00083-5

Breitel, D., Brett, P., Alseekh, S., Fernie, A. R., Butelli, E., & Martin, C. (2021). Metabolic engineering of tomato fruit enriched in L-DOPA. *Metabolic Engineering, 65*, 185–196. https://doi.org/10.1016/j.ymben.2020.11.011

Campuzano, A., Rosell, C. M., & Cornejo, F. (2018). Physicochemical and nutritional characteristics of banana flour during ripening. *Food Chemistry, 256*, 11–17. https://doi.org/10.1016/j.foodchem.2018.02.113

Chen, M., Huang, W., Yin, Z., Zhang, W., Kong, Q., Wu, S., … Yan, S. (2022). Environmentally-driven metabolite and lipid variations correspond to altered bioactivities of black wolfberry fruit. *Food Chemistry, 372*, Article 131342. https://doi.org/10.1016/j.foodchem.2021.131342

Dong, Y., Sonawane, P., Cohen, H., Polturak, G., Avivi, S., Rogachev, I., & Aharoni, A. (2020). High mass resolution, spatial metabolite mapping enhances the current plant gene and pathway discovery toolbox. *New Phytologist, 228*, 1986–2002. https://doi.org/10.1111/nph.16809

Dunn, W. B., Broadhurst, D., Begley, P., Zelena, E., Francis-McIntyre, S., Anderson, N., Brown, M., Knowles, J. D., Halsall, A., Haselden, J. N., Nicholls, A. W., Wilson, I. D., Kell, D. B., Goodacre, R., & The Human Serum Metabolome (HUSERMET) Consortium (2011). Procedures for large-scale metabolic profiling of serum and plasma using gas chromatography and liquid chromatography coupled to mass spectrometry. *Nature Protocols, 6*(7), 1060-1083. https://doi.org/10.1038/nprot.2011.335.

Ekesa, B., Nabuuma, D., Blomme, G., & Van den Bergh, I. (2015). Provitamin A carotenoid content of unripe and ripe banana cultivars for potential adoption in eastern Africa. *Journal of Food Composition and Analysis, 43*, 1–6. https://doi.org/10.1016/j.jfca.2015.04.003

Guo, Y.-F., Zhang, Y.-L., Shan, W., Cai, Y.-J., Liang, S.-M., Chen, J.-Y., … Kuang, J.-F. (2018). Identification of two transcriptional activators MabZIP4/5 in controlling aroma biosynthetic genes during banana ripening. *Journal of Agricultural and Food Chemistry, 66*(24), 6142–6150. https://doi.org/10.1021/acs.jafc.8b01435

Hölscher, D., Dhakshinamoorthy, S., Alexandrov, T., Becker, M., Bretschneider, T., Buerkert, A., … Swennen, R. L. (2014). Phenalenone-type phytoalexins mediate

resistance of banana plants (*Musa* spp.) to the burrowing nematode *Radopholus similis*. *Proceedings of the National Academy of Sciences, 111*(1), 105–110. https://doi.org/10.1073/pnas.1314168110

Heng, Z., Sheng, O., Huang, W., Zhang, S., Fernie, A. R., Motorykin, I., … Yan, S. (2019). Integrated proteomic and metabolomic analysis suggests high rates of glycolysis are likely required to support high carotenoid accumulation in banana pulp. *Food Chemistry, 297*, Article 125016. https://doi.org/10.1016/j.foodchem.2019.125016

Horikawa, K., Hirama, T., Shimura, H., Jitsuyama, Y., & Suzuki, T. (2019). Visualization of soluble carbohydrate distribution in apple fruit flesh utilizing MALDI–TOF MS imaging. *Plant Science, 278*, 107–112. https://doi.org/10.1016/j.plantsci.2018.08.014

Li, B., Ge, J., Liu, W., Hu, D., & Li, P. (2021). Unveiling spatial metabolome of *Paeonia suffruticosa* and *Paeonia lactiflora* roots using MALDI MS imaging. *New Phytologist, 231*, 892–902. https://doi.org/10.1111/nph.17393

Lima, G. P. P., Da Rocha, S. A., Takaki, M., Ramos, P. R. R., & Ono, E. O. (2008). Comparison of polyamine, phenol and flavonoid contents in plants grown under conventional and organic methods. *International Journal of Food Science & Technology, 43*(10), 1838–1843. https://doi.org/10.1111/j.1365-2621.2008.01725.x

Maduwanthi, S. D. T., & Marapana, R. A. U. J. (2021). Total phenolics, flavonoids and antioxidant activity following simulated gastro-intestinal digestion and dialysis of banana (*Musa acuminata*, AAB) as affected by induced ripening agents. *Food Chemistry, 339*, Article 127909. https://doi.org/10.1016/j.foodchem.2020.127909

Marriott, J., & Palmer, J. K. (1980). Bananas — physiology and biochemistry of storage and ripening for optimum quality. *Critical Reviews in Food Science and Nutrition, 13*(1), 41–88. https://doi.org/10.1080/10408398009527284

Mondal, A., Banerjee, S., Bose, S., Das, P. P., Sandberg, E. N., Atanasov, A. G., & Bishayee, A. (2021). Cancer preventive and therapeutic potential of banana and its bioactive constituents: A systematic, comprehensive, and mechanistic review. *Frontiers in Oncology, 11*, Article 697143. https://doi.org/10.3389/fonc.2021.697143

Nascimento, T. P., Castro-Alves, V. C., Castelan, F. P., Calhau, M. F. N. S., Saraiva, L. A., Agopian, R. G., & Cordenunsi-Lysenko, B. R. (2019). Metabolomic profiling reveals that natural biodiversity surrounding a banana crop may positively influence the nutritional/sensorial profile of ripe fruits. *Food Research International, 124*, 165–174. https://doi.org/10.1016/j.foodres.2018.07.050

Pareek, V., Tian, H., Winograd, N., & Benkovic, S. J. (2020). Metabolomics and mass spectrometry imaging reveal channeled de novo purine synthesis in cells. *Science, 368*(6488), 283–290. https://doi.org/10.1126/science.aaz6465

Pereira, A., & Maraschin, M. (2015). Banana (*Musa* spp) from peel to pulp: Ethnopharmacology, source of bioactive compounds and its relevance for human health. *Journal of Ethnopharmacology, 160*, 149–163. https://doi.org/10.1016/j.jep.2014.11.008

Qamar, S., & Shaikh, A. (2018). Therapeutic potentials and compositional changes of valuable compounds from banana- A review. *Trends in Food Science & Technology, 79*, 1–9. https://doi.org/10.1016/j.tifs.2018.06.016

Qin, R., Li, P., Du, M., Ma, L., Huang, Y., Yin, Z., … Wu, X. (2021). Spatiotemporal visualization of insecticides and fungicides within fruits and vegetables using gold nanoparticle-immersed paper imprinting mass spectrometry imaging. *Nanomaterials, 11*(5), 1327. https://doi.org/10.3390/nano11051327

Samarah, L. Z., Tran, T. H., Stacey, G., & Vertes, A. (2021). Mass spectrometry imaging of bio-oligomer polydispersity in plant tissues by laser desorption ionization from silicon nanopost arrays. *Angewandte Chemie International Edition, 60*(16), 9071–9077. https://doi.org/10.1002/anie.202015251

Sidhu, J. S., & Zafar, T. A. (2018). Bioactive compounds in banana fruits and their health benefits. *Food Quality and Safety, 2*(4), 183–188. https://doi.org/10.1093/fqsafe/fyy019

Singh, B., Singh, J. P., Kaur, A., & Singh, N. (2016). Bioactive compounds in banana and their associated health benefits – A review. *Food Chemistry, 206*, 1–11. https://doi.org/10.1016/j.foodchem.2016.03.033

Sun, C., Li, T., Song, X., Huang, L., Zang, Q., Xu, J., … Abliz, Z. (2019). Spatially resolved metabolomics to discover tumor-associated metabolic alterations. *Proceedings of the National Academy of Sciences, 116*(1), 52–57. https://doi.org/10.1073/pnas.1808950116

Sun, F., Chen, H., Chen, D., Tan, H., Huang, Y., & Cozzolino, D. (2020). Lipidomic changes in banana (*Musa cavendish*) during ripening and comparison of extraction by Folch and Bligh-Dyer methods. *Journal of Agricultural and Food Chemistry, 68*(40), 11309–11316. https://doi.org/10.1021/acs.jafc.0c04236

Valérie Passo Tsamo, C., Andre, C. M., Ritter, C., Tomekpe, K., Ngoh Newilah, G., Rogez, H., & Larondelle, Y. (2014). Characterization of *Musa* sp. fruits and plantain banana ripening stages according to their physicochemical attributes. *Journal of Agricultural and Food Chemistry, 62*(34), 8705–8715. https://doi.org/10.1021/jf5021939

Wang, T., Cheng, X., Xu, H., Meng, Y., Yin, Z., Li, X., & Hang, W. (2020). Perspective on advances in laser-based high-resolution mass spectrometry imaging. *Analytical Chemistry, 92*(1), 543–553. https://doi.org/10.1021/acs.analchem.9b04067

Wu, X., Qin, R., Wu, H., Yao, G., Zhang, Y., Li, P., … Xu, H. (2020). Nanoparticle-immersed paper imprinting mass spectrometry imaging reveals uptake and translocation mechanism of pesticides in plants. *Nano Research, 13*(3), 611–620. https://doi.org/10.1007/s12274-020-2700-5

Xiao, Z., Chen, H., Niu, Y., & Zhu, J. (2021). Characterization of the aroma-active compounds in banana (*Musa* AAA Red green) and their contributions to the enhancement of sweetness perception. *Journal of Agricultural and Food Chemistry, 69*(50), 15301–15313. https://doi.org/10.1021/acs.jafc.1c06434

Yan, S., Liu, Q., Naake, T., Huang, W., Chen, M., Kong, Q., … Liu, B. (2021). *OsGF14b* modulates defense signaling pathways in rice panicle blast response. *The Crop Journal, 9*(4), 725–738. https://doi.org/10.1016/j.cj.2020.10.007

Yap, M., Fernando, W. M. A. D. B., Brennan, C. S., Jayasena, V., & Coorey, R. (2017). The effects of banana ripeness on quality indices for puree production. *LWT, 80*, 10–18. https://doi.org/10.1016/j.lwt.2017.01.073

Yin, Z., Cheng, X., Liu, R., Li, X., Hang, L., Hang, W., … Tian, Z. (2019). Chemical and topographical single-cell imaging by near-field desorption mass spectrometry. *Angewandte Chemie International Edition, 58*(14), 4541–4546. https://doi.org/10.1002/anie.201813744

Yuan, Y., Zhao, Y., Yang, J., Jiang, Y., Lu, F., Jia, Y., & Yang, B. (2017). Metabolomic analyses of banana during postharvest senescence by 1H-high resolution-NMR. *Food Chemistry, 218*, 406–412. https://doi.org/10.1016/j.foodchem.2016.09.080

Yun, Z., Gao, H., Chen, X., Duan, X., & Jiang, Y. (2022). The role of hydrogen water in delaying ripening of banana fruit during postharvest storage. *Food Chemistry, 373*, Article 131590. https://doi.org/10.1016/j.foodchem.2021.131590